ICMIEE20-192

CFD Study on Aerodynamic Characteristics of a NACA 0012 Airfoil With and Without Flap

Md. Najmus Salehin, Fahim Islam Anik, Sadman Durlov, MD Arif Khan, MD Ikramul Hasib*
Department of Mechanical Engineering, Khulna University of Engineering & Technology, Khulna-9203, BANGLADESH

ABSTRACT
This paper concerns on the aerodynamic characteristic study of a 2D NACA 0012 airfoil with and without flap. Here in this research a NACA 0012 airfoil geometry without flap is generated with ANSYS DesignModeler Geometry using airfoil tool. The solver setup and solution is validated for 0^O, 10^O, 15^O angles of attack comparing with 2D NACA 0012 Airfoil Validation Case of NASA Langley Research Center's Turbulence Modeling Resource. Then an airfoil is generated with plain flaps with various flap angles (4^O, 8^O, 12^O, 16^O, 20^O). Different angles of attack are considered to compare the cases of flapped and no flapped airfoils. The aerodynamic behavior of both cases are compared in this paper. For this paper, Spalart-Allmaras turbulence model and an airfoil with chord length of 1m is used.

Keywords: Airfoil, flap, ANSYS, CFD analysis, Spalart-Allmaras turbulence model.

1. Introduction

An airfoil is basically the cross sectional geometry of any lifting or propelling device (i.e. wings, blades etc.). When a body with an airfoil shaped device or of a shape of an airfoil moves through fluid flow, lift and drag forces are generated which are exerted on the airfoil. The force component that work normal to the direction of motion is called lift force and the force component that works parallel to the motion is called drag force. A flap is a high lift device (HLD) which increased lift force. It also allows the pilot to control lift by the optimization of position and angle during flight. Different types of flaps have different effects on coefficient of lift (C_L).

NACA 0012 is a highly used airfoil. It is a highly worked on airfoil with well documented dataset provided by NASA [1] Langley Research Center. This study doesn't include experimental features, the data provided by Ladson et al [2] for R_e of 6 million is rather used to validate the computational method for no flap and 0^O, 10^O, 15^O angles of attack for NACA 0012 airfoil. Almost the same computational method is then used for flapped airfoils of different (4^O, 8^O, 12^O, 16^O, 20^O) flap angles.

For turbulence criteria, Spalart-Allmaras turbulence model is used in this study.

2. Background Study

For generating high lift and having maximum lifting efficiency high lift devices (HLD) are must in modern day aerospace industries. Various HLD's are flaps, slats and slots, leading edge root extensions, co-flow jet etc. most common type of HLD's are flaps. Various types of flaps are plain flap, split flap, slotted flap, double slotted flap etc. All the types of flaps develops lifting effects in different magnitude. The development of C_L is different for each.

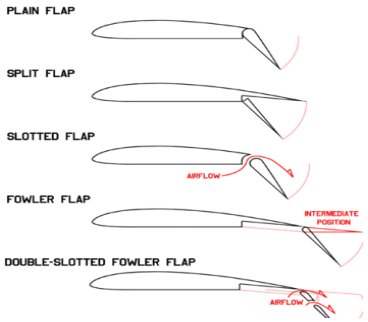

Fig. 1 Different types of flaps [3]

In changing from a plain airfoil to an airfoil with flaps an increase of curvature of the airfoil is featured which gives part of the extra lift, but also a depression is created which features a low pressure near the trailing edge. It creates a pull acting from the trailing edge that pulls the air around the leading edge which prevents the separation [4]

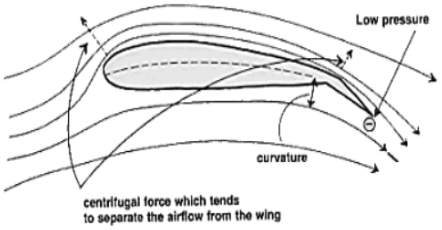

Fig. 2 Characteristics of streamlines over flapped airfoil [4]

With the increase of angle of attack, primarily C_L increased, but when maximum C_L is achieved, C_L starts decreasing because of stalling.

* Corresponding author. Tel.: +88-01909464570
E-mail addresses: sagar.salehin023@gmail.com

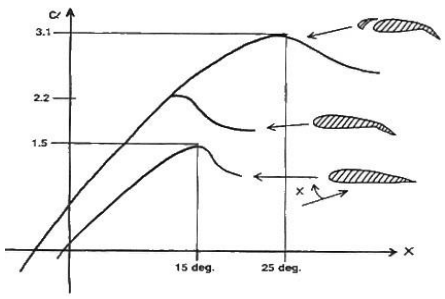

Fig. 3 Effects of HLD's on the lift curve [4]

2.1 Turbulence Model

The Spalart-Allmaras turbulence model is a one equation turbulence model which is basically prepared for external non complicated aerodynamic analysis. It features a transport equation for eddy viscosity. In order to develop a closed system of the central equation for the mean motion of a flow, one would determine the distribution of the Reynolds stress [5]. In a laminar flow problem like this turbulence model is needed for smoother transition between laminar and turbulent flow.

The working variable $\tilde{\nu}$ transport equation is given by,

$$\frac{\partial \tilde{\nu}}{\partial t} + \tilde{u_j}\frac{\partial \tilde{\nu}}{\partial x_j} = \underbrace{C_{b1}\tilde{S}\tilde{\nu}\frac{1}{\sigma}}_{Production} + \underbrace{\left[\frac{\partial}{\partial x_j}\left((\nu+\tilde{\nu})\frac{\partial \tilde{\nu}}{\partial x_j}\right)c_{b2}\frac{\partial \tilde{\nu}}{\partial x_j}\frac{\partial \tilde{\nu}}{\partial x_j}\right]}_{Diffusion} - \underbrace{c_{w1}f_{w1}\left(\frac{\tilde{\nu}}{d}\right)^2}_{Destruction} \quad (1)$$

$$\mu_t = \bar{\rho}\tilde{\nu}f_{v1} = \bar{\rho}\nu_t \quad (2)$$

In all three (log, buffer, viscous) layer,

$$\tilde{\nu} = kyu_\tau \quad (3)$$

In the transport equation,

$$f_{v1} = \frac{\chi^3}{\chi^3+c_{v1}} \quad \text{Where} \quad \chi = \frac{\tilde{\nu}}{\nu} \quad (4)$$

$$\tilde{S} = \sqrt{2\Omega_{ij}\Omega_{ij}}f_{v3} + \frac{\tilde{\nu}}{k^2d^2}f_{v2} \quad (5)$$

Where: $\Omega_{ij} = \frac{1}{2}\left(\frac{\partial \tilde{u_i}}{\partial x_j} - \frac{\partial \tilde{u_j}}{\partial x_j}\right)$; $f_{v2} = 1 - \frac{\chi}{1+\chi f_{v1}}$

and $f_{v3} = 1$

$$f_w(g) = g\left(\frac{1+c_{w3}^6}{g^6+c_{w3}^6}\right)^6 \quad (6)$$

Where: $g = r + c_{w2}(r^6 - r)$ and $r = \frac{\tilde{\nu}}{\tilde{S}k^2d^2}$

3. Computational Method

To compute and validate the solver scheme, a 2D NACA 0012 airfoil is generated with a little modification to close the trailing edge in online airfoil tool [6] of 1m in chord length with a farfield having 78570 nodes and 78000 elements. Fig. 4-5 shows the farfield and closed detail of the meshed farfield region with the airfoil. Here for boundary conditions are taken as a constant 88.65m/s (M_∞=0.258) air velocity, a constant 288.16 K temperature, a density of 1.225 kg/m^3 and viscosity of $1.81 \times 10^{-5}\ kg/ms$ (for R_e=6×10^6). Outlet condition is kept as pressure outlet type.

$$\mu = \frac{\rho u L}{R_e} = 1.81 \times 10^{-5}\ kg/ms$$

The biased edge sizing is used in mesh maintain a reasonable y^+. Hybrid initialization is used for computation.

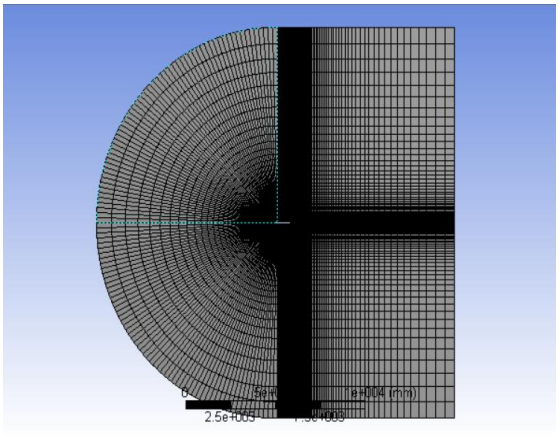

Fig. 4 Meshed farfield

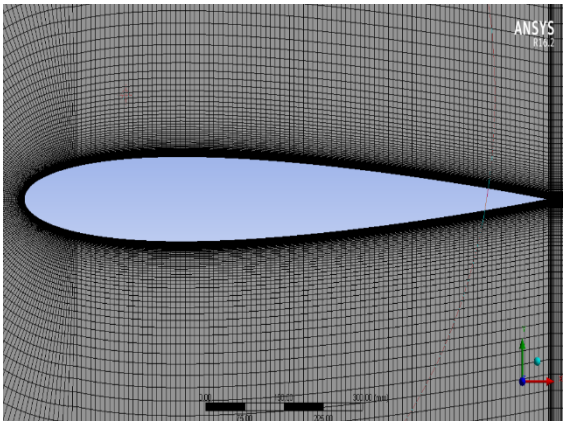

Fig. 5 Closed detail

4. Validation of the process

Data provided by Ladson et al [2] for C_p is used to validate the simulation method. The method primarily ran the computation for NACA 0012 with zero flap angle for angles of attack 0^O, 10^O, and 15^O. Then the C_p data is compared by overlapping on the curve generated by the Ladson et al [2] pressure data. Fig. 6-8 shows the comparison.

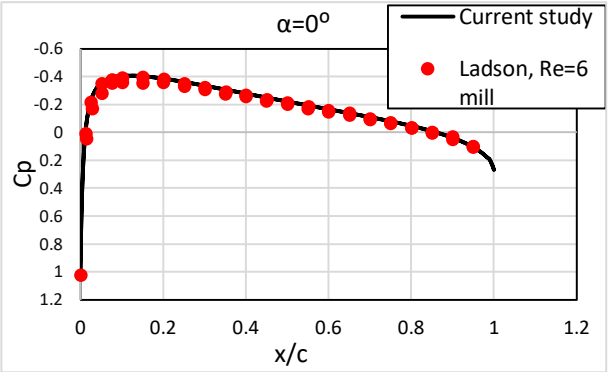

Fig. 6 Variation of C_p for $\alpha=0^O$

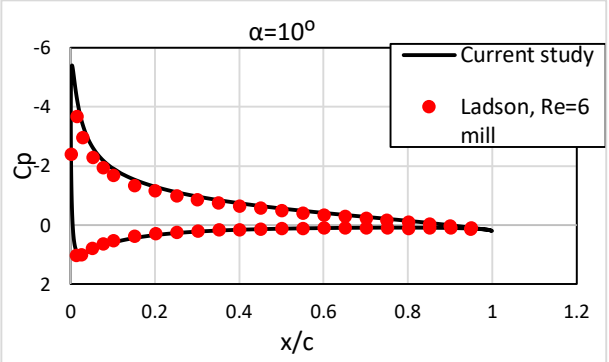

Fig. 7 Variation of C_p for $\alpha=10^O$

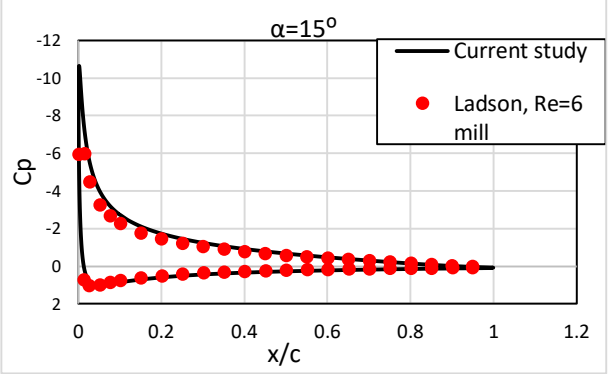

Fig. 8 Variation of C_p for $\alpha=15^O$

The figures 6, 7 and 8 shows that the current study's computational method is well synced with the Ladson et al [2] pressure data for $R_e=6\times10^6$, free transition for all three angles of attack (0^O, 10^O, 15^O). The slightest negligible deviation is occurred mainly because of unmatched surface roughness of the airfoil wall.

5. Result and Discussion

The generated airfoils with different flap angles (4^O, 8^O, 12°, 16° and 20°) and of the model NACA 0012 is simulated under different condition. The airflow is left as constant under Mach number smaller than 0.3 ($M_\infty=0.258$). The airfoil is subjected to this constant velocity air for different angles of attack (0°, 5°, 10°, 15° and 20°). As the flow is under 0.3 Mach, the flow can be considered as incompressible flow. So, a pressure based solver is used rather than a density based one. Spalart-Allmaras Eddy-Viscosity model is used which is a RANS (Reynolds-averaged Navier-Stokes) turbulence model to run and calculate the simulation.

5.1 Variation of C_p

Figures (9-11) shows the variation of the coefficient of pressure for different angles of attack for different flap angles. The C_p curves show a little distortion near the trailing edge (at x/c=0.7638) because of the position of flaps. The upper surface is subjected to negative pressure which causes the suction effect caused by the lower pressure in the trailing edge because of the existence of flap. The lower surface however is subjected to positive pressure. The negative (suction) pressure gradually increases with the increase of angle of attack up to 15 degree, starts to drop with farther increase of angle of attack because of stalling effect.

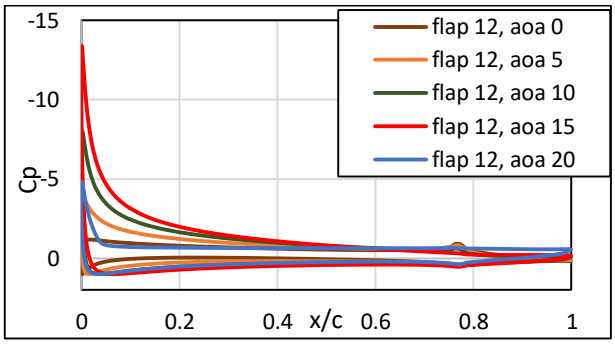

Fig. 9 Variation of C_p for flap angle=12^O

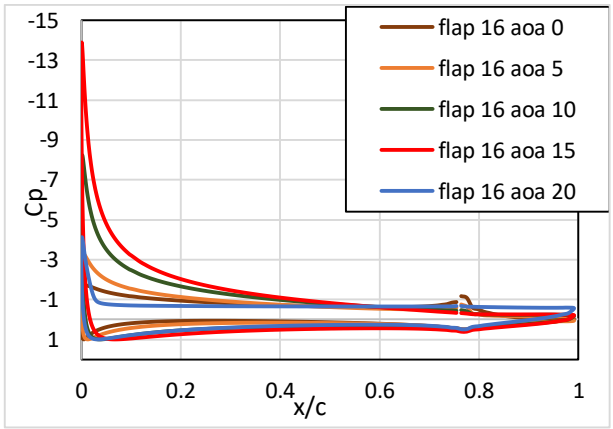

Fig. 10 Variation of C_p for flap angle=16^O

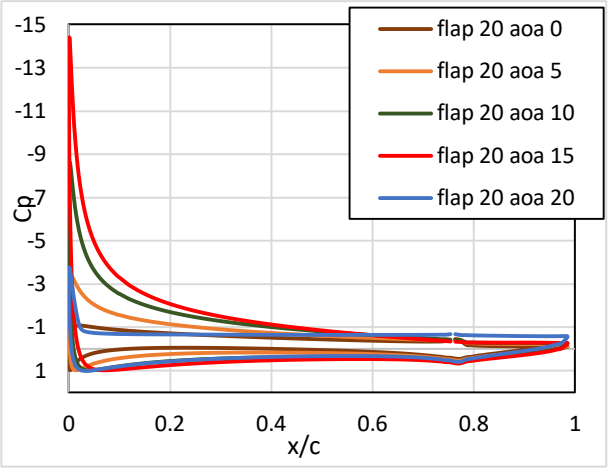

Fig. 11 Variation of C_p for flap angle=20^O

5.2 Variation of C_L

Figure 12 shows the variations of lift coefficient with angle of attack (lift curves) for different flap angles (4^O, 8^O, 12°, 16° and 20°) and for no flap condition as well. It shows that the flapped airfoils generate higher lifts than the airfoil without flap and the higher the flapped angle is, the higher the generated lifts are. The trailing edge flap basically move downwards and increases the effective camber which causes the increase of maximum lift. It also decreases the stalling angle of attack. The lift curved dives downwards because of stall for higher angles of attack. Stalling occurs due to boundary layer retardation and flow separation for higher angles of attack.

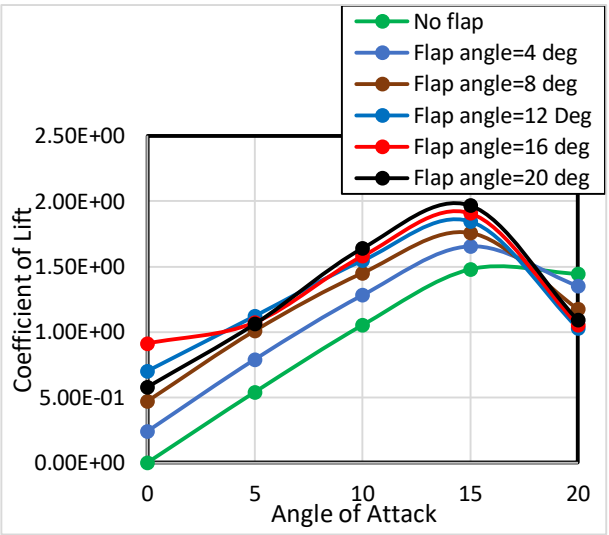

Fig. 12 Lift Curves

5.3 Velocity contour

Figures (13-20) shows the velocity contours around the airfoil for intermediate angles of attack (5°, 10°, 15°). The velocity contours clearly depicts velocity increasing and decreasing in certain points. The higher velocity regions have lower pressure and vice versa according to Bernoulli's principle. It is seen that the flow separation region is longer for higher angle of attack.

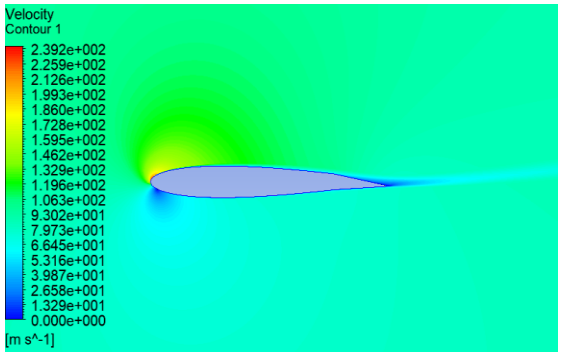

Fig. 13 Velocity contour for δ=4°, α=10°

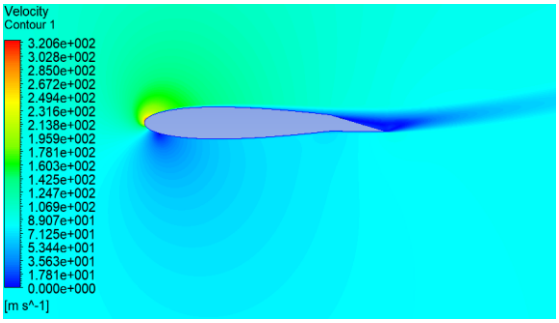

Fig. 14 Velocity contour for δ=8°, α=15°

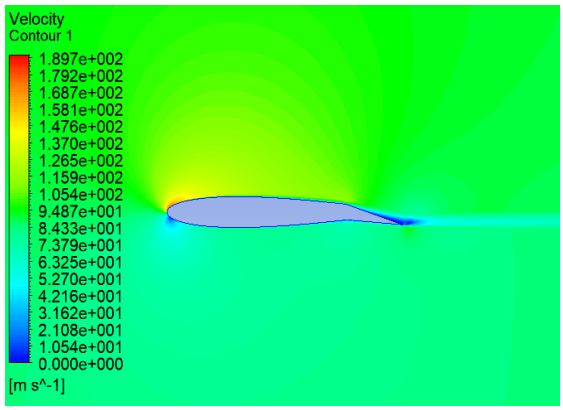

Fig. 15 Velocity contour for δ=12°, α=5°

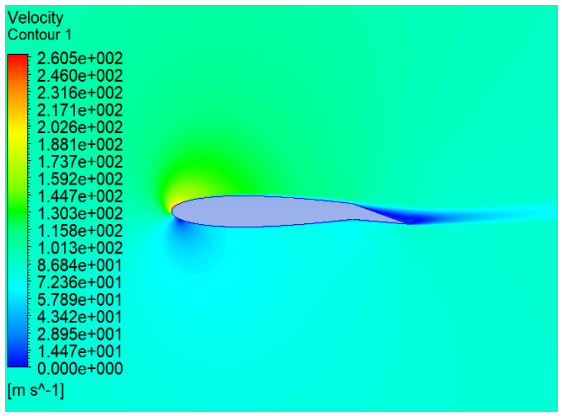

Fig. 16 Velocity contour for δ=12°, α=10°

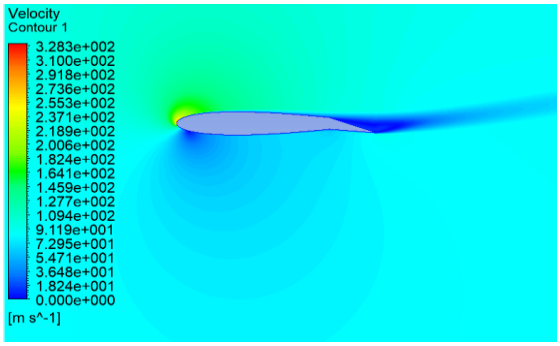

Fig. 17 Velocity contour for δ=12°, α=15°

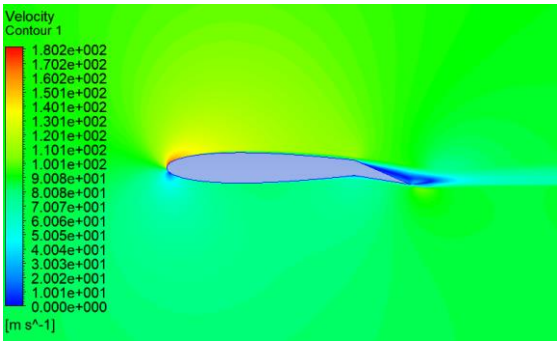

Fig. 18 Velocity contour for δ=16°, α=5°

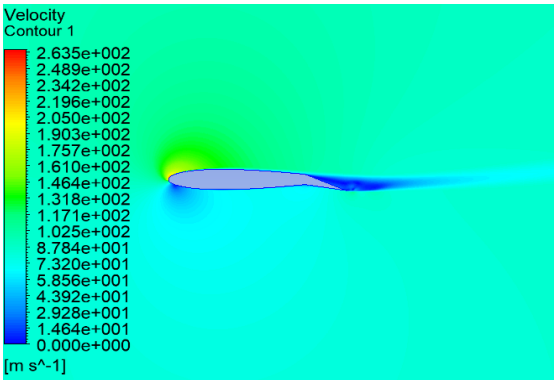

Fig. 19 Velocity contour for δ=16°, α=10°

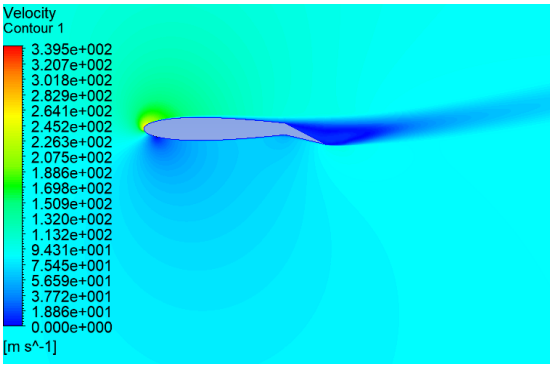

Fig. 20 Velocity contour for δ=20°, α=15°

Figures 13 shows that at moderate AoA and low δ, velocity deviation around is not very significant. In fig 15 at higher δ, the deviation is also low with lower AoA. In fig 14 deviation is higher with intermediate δ and higher AoA. In figs 16 and 17 significant changes happens with the change of AoA for δ=12 degree. In 18 and 19 again significant changes noticed for same δ and different AoA. Fig 20 shows a larger flow separation for high δ and high AoA. Figure 21 shows the stalling condition for 16 degree flap angle at higher (20 degree) angle of attack. It depicts a much bigger flow separation region. Observation indicates for lower δ change of AoA dominates the velocity deviations.

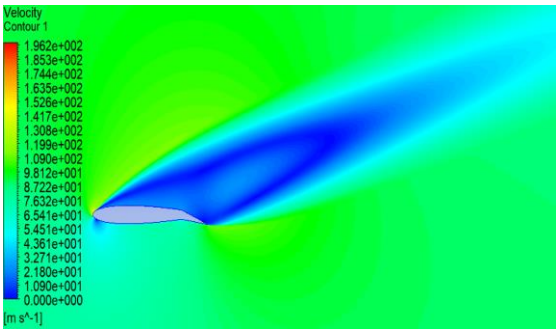

Fig. 21 Velocity contour for δ=16°, α=20°

5.4 Pressure Contours

Figures (22-26) shows the pressure contour for low and high flapped airfoils for 15 degree angle of attack where maximum lift occurs for each. It is seen that the low velocity regions having high pressure and high velocity regions having low pressure.

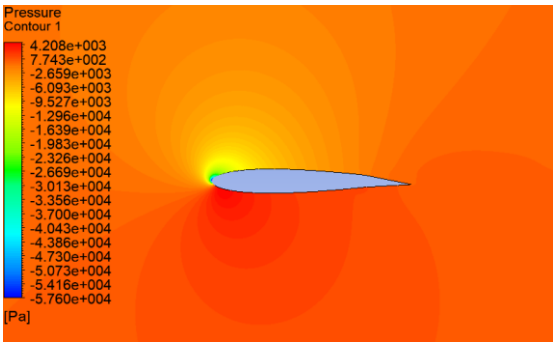

Fig. 22 Pressure contour for δ=4°, α=15°

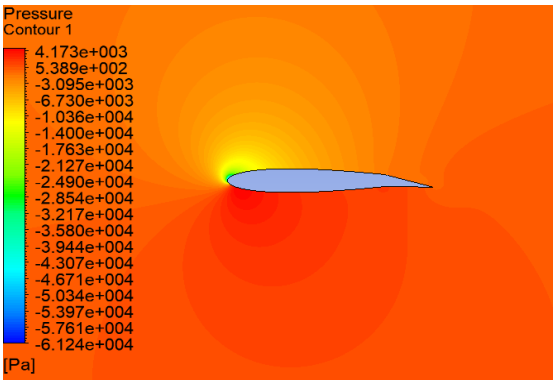

Fig. 23 Pressure contour for δ=8°, α=15°

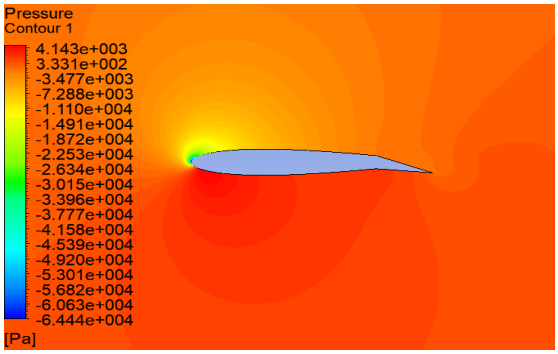

Fig. 24 Pressure contour for δ=12°, α=15°

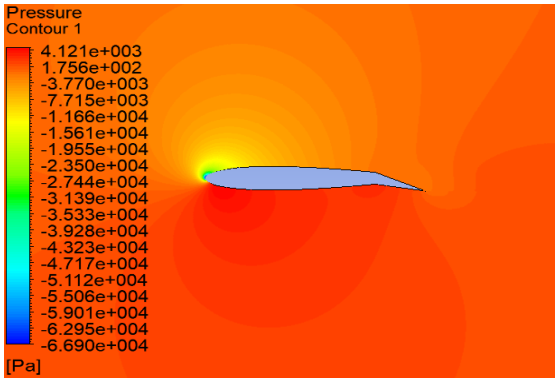

Fig. 25 Pressure contour for δ=16°, α=15°

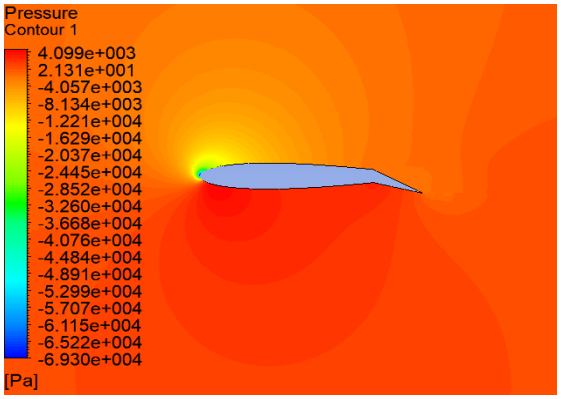

Fig. 26 Pressure contour for δ=20°, α=15°

All figures 22, 23, 24, 25, 26 are pressure contours for AoA=15 and δ=4, 8, 12, 16 and 20, here it is observed that for the change of δ for same AoA changes of pressure is quite insignificant for consecutive changes, so, change of AoA is more significant factor in both velocity and pressure changes.

6. Conclusion

In this study the aerodynamic behavior of 2D NACA 0012 profiles with flaps is observed and compared with the no flap condition. The calculation method is validated with data provided by NASA [1]. The provided data and the current study data are well convenient as negligible amount of error noticed. It is seen that for high flap angles, high lift is achieved, also stalling angle is decreased, normally flap angles 5-15 degree is considered for takeoff condition. But wings having high flap angles also have speed limitations during takeoff as angle of attack is higher during takeoff. The current study can inspire the amount flap angle and stalling conditions to be taken under good consideration.

8. References

[1] NASA Langley Research Center, "2D NACA 0012 Airfoil Validation," *Turbulence Modeling Resource*, 2019. [Online]. Available: https://turbmodels.larc.nasa.gov/naca0012_val.html. [Accessed: 23-Jul-2020].

[2] C. L. Ladson, W. G. Johnson, and A. S. Hill, "Pressure Distributions From High Reynolds Number Tests of a Boeing Bac I Airfoil in the Langley 0. 3-Meter Transonic Cryogenic Tunnel.," 1985.

[3] "File:Flap types.png - SKYbrary Aviation Safety," 2013. [Online]. Available: https://www.skybrary.aero/index.php/File:Flap_types.png. [Accessed: 23-Jul-2020].

[4] C. Heintz, "Airfoils, Part 3," *EAA Light Plane World magazine*, 1987. [Online]. Available: http://www.zenithair.com/kit-data/ht-87-8.html. [Accessed: 23-Jul-2020].

[5] Č. Kostić, "Review of the Spalart-Allmaras turbulence model and its modifications to three-dimensional supersonic configurations," *Sci. Tech. Rev.*, vol. 65, no. 1, pp. 43–49, 2016.

[6] AirfoilTools.com, "NACA 0012 AIRFOILS (n0012-il)," *Online Source*, 2013. [Online]. Available: http://airfoiltools.com/airfoil/details?airfoil=n0012-il. [Accessed: 23-Jul-2020].

NOMENCLATURE

μ_t :eddy viscosity, Pa-s
ρ :density, Kg/m^3
υ :kinematic viscosity, m^2-s
μ :dynamic viscosity, Pa-s
Ω : shear rate tensor
d :distance from the field point to nearest wall, m
f_{v1} :damping function
C_p :coefficient of pressure
C_L : coefficient of lift
M_∞ : mach number
R_e : Reynolds number
x : x axial position in the airfoil, m
c : chord length, m
α : angle of attack, degree
δ :flap angle, degree
i,j,k :cartesian unit vector